Electron-Wavepacket Reaction Dynamics in Proton Transfer of Formamide†

Kengo Nagashima and Kazuo Takatsuka*

Department of Basic Science, Graduate School of Arts and Sciences, University of Tokyo, Komaba, 153-8902 Tokyo, Japan

Received: June 15, 2009; Revised Manuscript Received: August 4, 2009

We apply the semiclassical Ehrenfest theory, which provides electron wavepacket dynamics coupled to nuclear motion, to a study of water-assisted proton relay in formamide compared with a forced proton transfer in gas phase, both of which are associated with the tautomerization. We start with the enol (imidic acid) form HO−CH═NH and track its proton transfer process to the keto (amide) form O═CH−NH_2. Identifying the fact that this is indeed a "proton transfer process" rather than hydrogen-atom migration in terms of radical character on the proton, we show a collective quantum flux of electrons, which flows backward against the proton motion. This backward flux compensates the electrons tightly covering the proton, as represented in the Mulliken charge. The enol form formamide is one of the simplest species in the group O═CR_1−NHR_2, which is a unit of polypeptide. In the gas phase, the nitrogen atom may have a pyramidal structure as in the ammonium molecule; therefore, the C−N bond may allow low barrier rotation along it. This rotation is strongly prohibited by the formation of the double bond C═N induced by the proton transfer. Not only the dynamical process of proton transfer itself but also the electronic structures left behind are greatly affected by the presence of water molecule(s) and polar solvents. In discussing the relative stability of the formamide after the proton transfer, the following resonance structures are frequently mentioned, O^-−CH═N^+H_2 ↔ O═CH−NH_2. Here we address the dynamical manifestation of the resonance structures in terms of our dynamical electron theory.

1. Introduction

Chemical reaction dynamics is usually a synonym for studying the nuclear motion of molecules in the rearrangement collision, which is driven by the electronic energy along with the nuclear repulsion. It is treated in terms of quantum, semiclassical, and classical mechanics depending on the mass and energy scales within the grand scheme of Born−Oppenheimer view:[1] The electronic states are treated as a stationary wave subject to the electronic Hamiltonian, and consequently, they are free of the time variable. The time scale of nuclear motion on such static potential energy hypersurfaces is typically 10−1000 fs in elementary chemical reactions. Great progress has been achieved in these studies, and in particular, Aquilanti has long been leading chemical reaction dynamics both theoretically and experimentally.[2,3]

In this article, we take another route to approach the essence of the dynamics of chemical reaction: We track the dynamics of electron wavepackets along a reaction path, which are driven adiabatically or nonadiabatically by nuclear motions. The electron dynamics is much faster than that of nuclear motion, whose time scale is typically as short as 10−1000 attoseconds. Even with the latest laser technology[4−15] in which the pulse width is as short as 100 attoseconds or is intense beyond the order of 10^{16} W/cm^2, the direct monitoring of electron wavepacket dynamics is not yet possible. Nevertheless, it is very important to develop such a chemical reactivity theory within the realm of dynamical electrons.

As a case study, we pick "proton" transfer accompanied by tautomerization (shift of the position of double bonds) for the reason of their nuclear−electronic coupled dynamics. Through our systematic studies of proton transfer dynamics in formic acid dimer,[16] Zundel cation,[17] 5-methyl tropolone,[18] and so on, we have been puzzled by the following questions: (1) The Mulliken charge on the relevant "proton(s)" is almost constant through the entire course of transfer.[17] This implies that the proton is always covered by a certain amount of electrons, typically as much as 0.6 to 0.8 electrons. Therefore, it is not always trivial to judge whether the process is "(electron-rich) proton transfer" or "(electron-deficient) hydrogen-atom migration. (2) If it is proton transfer, then how can the covering electrons be compensated, and what is the pathway of electron back-transfer? These questions cannot be essentially resolved by means of the so-called AIMD (ab initio molecular dynamics method) or its variants[19] because the electronic eigenfunctions in the Born−Oppenheimer approximation do not contain the time variable.[20] We therefore use a theory of electron wavepacket that is synchronized with nuclear motion.

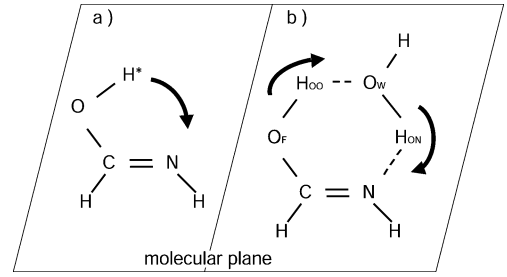

Figure 1. (a) Forced proton transfer of formamide in gas phase. (b) Relayed proton transfer mediated by a water molecule (water-assisted proton transfer). The proton transfer is associated with tautomerization from the enol form HO−CH═NH to the keto form O═CH−NH_2.

In this article, we study water-assisted (relayed) proton transfer in formamide, compared with a forced proton transfer within formamide in the gas phase (Figure 1), which is also associated with the tautomerization. We start from the enol

† Part of the "Vincenzo Aquilanti Festschrift".

* Corresponding author. E-mail: kaztak@mns2.c.u-tokyo.ac.jp.

10.1021/jp905583s
Published on Web 10/09/2009

(imidic acid) form HO−CH═NH and track the transfer process to the keto (amide) form O═CH−NH_2. We first survey the above very basic puzzles with this system, identifying the fact that this is indeed a "proton transfer process" in terms of the spatial distribution of radicals (unpaired electron density)[21] on the transferring proton. Then, we show a collective electron quantum flux of electrons, which flows backward against the proton motion, thereby suggesting the compensation of tightly covering the proton, as represented in terms of the Mulliken charge. Besides these basic issues, this molecular system is of a particular relevance to protein dynamics. The keto form formamide is one of the simplest species in the group O═CR_1−NHR_2, which is a unit of polypeptide. In the gas phase, the nitrogen atom can have a pyramidal structure as in ammonium molecule; therefore, the C−N bond may allow free (low barrier) rotation along it. This rotation is obviously prohibited by the formation of the double bond C═N induced by the proton transfer. Not only the proton transfer itself, which we confirm that this process is indeed the case, but also the electronic structures left behind are greatly affected by the presence of water molecule(s) and polar solvents. In discussing the relative stability of the formamide after the proton transfer, the resonance structures O^-−CH═N^+H_2 ↔ O═CH−NH_2 are usually considered. Although there is no need to emphasize the fact that the Pauling resonance theory is extremely useful and constitutes a basic language of chemistry, here we revisit it to reveal the dynamical manifestation of the present resonance structures a little deeper in terms of our dynamical electron theory.

The present article is organized as follows. In Section 2, we first present the method and quantities we use in the analysis of the proton transfer dynamics. Section 3 identifies the mechanism of the present proton-transfer dynamics and shows how the electron flow is induced within the molecular system. Also, we consider the dynamical reality of the Pauling resonance structures appearing in the present dynamics. The article concludes in Section 4.

2. Methods of Computation and Analysis

2.1. Semiclassical Ehrenfest Theory to Track Electron Wavepacket Dynamics. One of the most powerful methods for studying the nonadiabatic transition starts from a time-dependent electronic Schrödinger equation

$$i\hbar\frac{\partial}{\partial t}\Phi_I(\mathbf{r};\mathbf{R}(t)) = H^{(\mathrm{el})}(\mathbf{r};\mathbf{R}(t))\Phi_I(\mathbf{r};\mathbf{R}(t)) \tag{1}$$

which seemingly appears to be a naive generalization of the stationary-state electronic Schrödinger equation of fixed nuclei approximation. This method is widely called the semiclassical Ehrenfest theory (SET).[22,23,15] The associated total wave function is assumed to have the form (unnormalized)

$$\Psi(\mathbf{r},\mathbf{R},t) = \sum_{\mathrm{path}} \Phi(\mathbf{r};\mathbf{R}_{\mathrm{path}}(t))\delta(\mathbf{R} - \mathbf{R}_{\mathrm{path}}(t)) \tag{2}$$

where the electronic wavepacket propagated along a path $\mathbf{R}_{\mathrm{path}}(t)$ is expanded as

$$\Phi(\mathbf{r};\mathbf{R}_{\mathrm{path}}(t)) = \sum_I C_I(t)\Phi_I(\mathbf{r};\mathbf{R})|_{\mathbf{R}=\mathbf{R}_{\mathrm{path}}(t)} \tag{3}$$

with the coefficients being supposed to satisfy the coupled electronic time-dependent Schrödinger equations

$$i\hbar\frac{\partial}{\partial t}C_I = \sum_J \left[H_{IJ}^{(\mathrm{el})} - i\hbar\sum_k \dot{R}_k X_{IJ}^k - \frac{\hbar^2}{4}\sum_k (Y_{IJ}^k + Y_{JI}^{k*})\right]C_J \tag{4}$$

where

$$X_{IJ}^k = \left\langle \Phi_I \middle| \frac{\partial \Phi_J}{\partial R_k} \right\rangle, \quad Y_{IJ}^k = \left\langle \Phi_I \middle| \frac{\partial^2 \Phi_J}{\partial R_k^2} \right\rangle \tag{5}$$

In the standard SET, the terms $-(\hbar^2/4)\Sigma_k(Y_{IJ}^k + Y_{JI}^{k*})$ are not included in eq 4. (Refer to refs 24−26 for the correction terms to the SET.) We also neglect these terms in this article for the usual reason that they contain $\hbar^2$.

The nuclear "classical" path carrying the electronic wavepacket is assumed to be driven by the mean force, that is[23]

$$\ddot{\mathbf{R}}_k(t) = -\sum_{I,J} C_I(t)^* C_J(t)\left(\sum_K [X_{IK}^k H_{KJ}^{(\mathrm{el})} - H_{IK}^{(\mathrm{el})} X_{KJ}^k] + \frac{\partial H_{IJ}^{(\mathrm{el})}}{\partial R_k}\right) \tag{6}$$

or if the basis set used was complete, then it holds that

$$\begin{aligned}\ddot{\mathbf{R}}_k(t) &= -\left\langle \Phi(\mathbf{R}_{\mathrm{path}}(t)) \middle| \frac{\partial H^{(\mathrm{el})}}{\partial \mathbf{R}} \middle| \Phi(\mathbf{R}_{\mathrm{path}}(t)) \right\rangle \\ &= -\sum_{I,J} C_I(t)^* C_J(t) \left\langle \Phi_I(\mathbf{R}_{\mathrm{path}}) \middle| \frac{\partial H^{(\mathrm{el})}}{\partial R_k} \middle| \Phi_J(\mathbf{R}_{\mathrm{path}}) \right\rangle\end{aligned} \tag{7}$$

which is a mathematical analog of the Hellmann−Feynman force.

The SET is not the best method to date[25,26] because after the resultant path passes across an avoided crossing region, it runs on an average path (in a mean-field) without reproducing branching paths.[22] However, it has been proven that SET gives a very good representation of the electron wavepacket as long as it is utilized within its validity range.[15,25,26]

2.2. Selected Quantities to Monitor the Dynamical Reactivity. We prepare a couple of theoretical quantities in advance to analyze the electron wavepacket dynamics to be studied in the next section.

2.2.1. Electron Density and Related Quantities. We begin with the spin-free reduced density matrix, which is defined as

$$\begin{aligned}\gamma(\mathbf{r}',\mathbf{r};t) = N\int \Phi^*(\mathbf{r}',\sigma_1,\mathbf{q}_2,...,\mathbf{q}_N;\mathbf{R}_{\mathrm{path}}(t)) \times \\ \Phi(\mathbf{r},\sigma_1,\mathbf{q}_2,...,\mathbf{q}_N;\mathbf{R}_{\mathrm{path}}(t))\, \mathrm{d}\sigma_1\, \mathrm{d}\mathbf{q}_2...\mathrm{d}\mathbf{q}_N\end{aligned} \tag{8}$$

where the four-vector $\mathbf{q}_i$ for the ith electron is a pair of the coordinates in configuration and spin space, $(\mathbf{r}_i,\sigma_i)$. The diagonal element $\gamma(\mathbf{r};t) \equiv \gamma(\mathbf{r},\mathbf{r};t)$ is just the electron density. In chemical applications, it is often expanded in atomic orbitals $\chi_{aA}(\mathbf{r})$ as

$$\gamma(\mathbf{r},t) = \sum_A \sum_a^{\text{on } A} \sum_B \sum_b^{\text{on } B} \rho_{aA,bB}(t)[\chi_{aA}(\mathbf{r})\chi_{bB}(\mathbf{r})] \tag{9}$$

where A and a represent an atom and the ath function on A, respectively, with $\rho_{aA,bB}(t)$ being the associated coefficient. The Mulliken population on an atom A is

$$M_A(t) = \sum_{a,a'}^{\text{on } A} \rho_{aA,a'A}(t) S_{aA,a'A} + \frac{1}{2} \sum_{a}^{\text{on } A} \sum_{B \neq A} \sum_{b}^{\text{on } B} \rho_{aA,bB}(t) S_{aA,bB} \tag{10}$$

where $S_{aA,bB}$ is the overlap integral between $\chi_{aA}(\mathbf{r})$ and $\chi_{bB}(\mathbf{r})$.

By extracting from $\gamma(\mathbf{r};t)$ only the product terms between the atomic orbitals belonging to two different atoms, say A and B, one can define the bond-order density in such a way

$$B_{AB}(\mathbf{r}, t) = \sum_{a}^{\text{on } A} \sum_{b}^{\text{on } B} \rho_{aA,bB}(t) [\chi_{aA}(\mathbf{r}) \chi_{bB}(\mathbf{r})] \tag{11}$$

The positiveness of its spatial distribution represents a formation of chemical bonding. The familiar bond order itself is recovered by integrating $B_{AB}(\mathbf{r},t)$ over $\mathbf{r}$.

It is well known that even the spin singlet ground state can have a biradical character due to electron correlation. To monitor the distribution of such radicals or unpaired electrons at a given site $\mathbf{r}$, we use the so-called unpaired electron density,[21] which is defined as

$$D(\mathbf{r}) = 2\gamma(\mathbf{r}, \mathbf{r}) - \int \mathrm{d}\mathbf{r}' \, \gamma(\mathbf{r}, \mathbf{r}') \gamma(\mathbf{r}', \mathbf{r}) \tag{12}$$

where γ $(\mathbf{r},\mathbf{r}')$ is an off-diagonal element of the first-order spin-free density matrix. $D(\mathbf{r})$ is represented in an invariant manner by means of the natural orbitals $\{\lambda_i(\mathbf{r})\}$, which diagonalize γ $(\mathbf{r},\mathbf{r}')$, as

$$D(\mathbf{r}) = \sum_i (2 - n_i) n_i |\lambda_i(\mathbf{r})|^2 \tag{13}$$

where n_i is the occupation number of $\lambda_i(\mathbf{r})$. It is obvious from this expansion that $n_i = 1$ maximizes $(2 - n_i)n_i$, and $n_i = 2$ (double occupancy) and $n_i = 0$ (vacancy) make null contribution to $D(\mathbf{r})$. Therefore, it is natural to define the spatial distribution of "radicals" using $D(\mathbf{r})$. When applied to chemical reaction in a singlet state, $D(\mathbf{r})$ can also distinguish its reaction mechanism, concerted reaction (with low unpaired electrons), or radical reactions (with high values) in a quantitative manner. It is straightforward to define the unpaired electron density on an atom A, say D_A, by expanding $D(\mathbf{r})$ in atomic basis functions as

$$D(\mathbf{r}) = \sum_{A,B}^{\text{atoms}} \sum_{a}^{\text{on } A} \sum_{b}^{\text{on } B} D_{aA,bB} [\chi_{aA}(\mathbf{r}) \chi_{bB}(\mathbf{r})] \tag{14}$$

The number of unpaired electrons on atom A, say D_A, is defined as

$$D_A = \sum_{a,a'}^{\text{on } A} D_{aA,a'A}(t) S_{aA,a'A} + \frac{1}{2} \sum_{a}^{\text{on } A} \sum_{B \neq A} \sum_{b}^{\text{on } B} D_{aA,bB}(t) S_{aA,bB} \tag{15}$$

(We will report a detailed account of the theory along with several examples in our future publication.[27])

2.2.2. Electron Flux. Let

$$i\hbar \frac{\partial}{\partial t} \psi(\mathbf{r}, t) = \left[-\frac{\hbar^2}{2m} \nabla^2 + V(\mathbf{r}, t) \right] \psi(\mathbf{r}, t) \tag{16}$$

be a one-body Schrödinger equation and consider a population loss from a closed volume Ω such that

$$\frac{\partial}{\partial t} \int_\Omega \psi^*(\mathbf{r}, t) \psi(\mathbf{r}, t) \, \mathrm{d}\mathbf{r} \tag{17}$$

then the flux vector naturally arises as[28]

$$\vec{j}(\mathbf{r}, t) = \frac{\hbar}{2im} [\psi^*(\mathbf{r}, t) \vec{\nabla} \psi(\mathbf{r}, t) - \psi(\mathbf{r}, t) \vec{\nabla} \psi^*(\mathbf{r}, t)] \tag{18}$$

This is a direct consequence of the conservation of probability and is automatically followed by the N-particle extension. With

$$\vec{\nabla}_N = \sum_{j=1}^{N} \left(\frac{\partial}{\partial x_j} \quad \frac{\partial}{\partial y_j} \quad \frac{\partial}{\partial z_j} \right) \tag{19}$$

the 3D flux is represented as

$$\vec{j}_N(\mathbf{r}_1, \mathbf{r}_2, ..., \mathbf{r}_N) = \frac{\hbar}{2im} (\psi^*(t) \vec{\nabla}_N \psi(t) - \psi(t) \vec{\nabla}_N \psi^*(t)) \tag{20}$$

which is reduced to the one-particle reduced flux

$$\vec{j}(\mathbf{r}_1) = N \int \vec{j}_N(\mathbf{r}_1, \mathbf{r}_2, ..., \mathbf{r}_N) \, \mathrm{d}\mathbf{r}_2 ... \mathrm{d}\mathbf{r}_N \tag{21}$$

or

$$\vec{j}(\mathbf{r}) = \frac{\hbar}{2im} \left[\vec{\nabla}_1 \gamma(\mathbf{r}', \mathbf{r}; t) - \vec{\nabla}_1 \gamma(\mathbf{r}, \mathbf{r}'; t) \right]_{\mathbf{r}'=\mathbf{r}} \tag{22}$$

where $\gamma(\mathbf{r}',\mathbf{r};t)$ is the off-diagonal spin-free first-order reduced density matrix.[29] In this expression, $\vec{\nabla}_1$ is to be operated on the $\mathbf{r}$ coordinates first; after that, $\mathbf{r}'$ should be replaced with $\mathbf{r}$. Okuyama and Takatsuka have recently shown how the electron flux induced by nuclear motion can be used to analyze chemical events.[20]

2.2.3. Time Fluctuation of the Electron Density. In an analysis using the electron flux, we sometimes face a situation in which the driving force causing the flux is not clear. In such a case, it is helpful to study the time-dependent local change of the electron density. We quantify such increasing or decreasing of the electron density at $\mathbf{r}$ as follows. First, we expand the instantaneous density matrix of the electronic state $\gamma(\mathbf{r},t;\mathbf{R})$ at each nuclear position in "molecular orbitals" $\phi_i(\mathbf{r};\mathbf{R})$ (not the atomic orbitals) such that

$$\gamma(\mathbf{r}, t; \mathbf{R}(t)) = \sum_{i,j} P_{ij}(t) \phi_i(\mathbf{r}; \mathbf{R}) \phi_j(\mathbf{r}; \mathbf{R})|_{\mathbf{R}=\mathbf{R}(t)} \tag{23}$$

where the coefficients $P_{ij}(t)$ are the function of the coefficient of CSF. It is

$$P_{ij}(t) = \langle \Phi(t)| \sum_{\sigma} \hat{X}^{\dagger}_{\sigma i} \hat{X}_{\sigma j} |\Phi(t)\rangle = \sum_{I,J} C^{*}_{I}(t) A^{ij}_{IJ} C_{J}(t) \tag{24}$$

where

$$A^{ij}_{IJ} = \langle \Phi_I| \sum_{\sigma} \hat{X}^{\dagger}_{\sigma i} \hat{X}_{\sigma j} |\Phi_J\rangle \tag{25}$$

with $\hat{X}^{\dagger}_{\sigma i}$ and $\hat{X}_{\sigma i}$ being the creation and annihilation operators, respectively, of an MO i of spin σ. We then consider the time derivative of γ, that is

$$\frac{\partial}{\partial t}\gamma(\mathbf{r}, t;\mathbf{R}) \equiv \sum_{i,j} \dot{P}_{ij}(t) \phi_i(\mathbf{r};\mathbf{R}) \phi_j(\mathbf{r};\mathbf{R}) \tag{26}$$

It should be noted that we take into account only the time derivative of $P_{ij}(t)$, whereas the derivative arising from $\partial \mathbf{R}(t)/\partial t$ is discarded. This is because we want to see only the electronic change due to the variation of chemical bonding, which is directly represented in $P_{ij}(t)$. (Note that the change of the electron density emerging from a simple shift of atomic position is not necessarily of direct relevance. For instance, suppose a translational motion of a free hydrogen atom, which necessarily causes the (trivial) spatiotemporal change of the electron density.) $\dot{P}_{ij}(t)$ can be estimated as follows. With the help of eq 4, we have

$$\begin{aligned} \dot{P}_{ij} &= \sum_{I,J} \dot{C}^{*}_{I} A^{ij}_{IJ} C_J + C^{*}_{I} A^{ij}_{IJ} \dot{C}_J \\ &= \sum_{I,J,K} \frac{i}{\hbar} C^{*}_{I} [(H^{\mathrm{el}}_{IK} + G^{\mathrm{cp}}_{IK}) A^{ij}_{KJ} - A^{ij}_{IK} (H^{\mathrm{el}}_{KJ} + G^{\mathrm{cp}}_{KJ})] C_J \end{aligned} \tag{27}$$

where

$$G^{\mathrm{cp}}_{IJ} = -i\hbar \sum_{k} \dot{R}_k X^{k}_{IJ} - \frac{\hbar^2}{4} \sum_{k} (Y^{k}_{IJ} + Y^{k*}_{JI}) \tag{28}$$

Neglecting the term proportional to $\hbar^2$ in G^{cp}_{IJ}, as usual, as

$$G^{\mathrm{cp}}_{IJ} \simeq -i\hbar \sum_{k} \dot{R}_k X^{k}_{IJ} \tag{29}$$

we obtain

$$\begin{aligned} \dot{P}_{ij} = \frac{i}{\hbar} \sum_{I,J,K} C^{*}_{I} [H^{\mathrm{el}}_{IK} A^{ij}_{KJ} - A^{ij}_{IK} H^{\mathrm{el}}_{KJ}] C_J + \\ \sum_{I,J,K} C^{*}_{I} [\sum_{k} \dot{R}_k (X^{k}_{IK} A^{ij}_{KJ} - A^{ij}_{IK} X^{k}_{KJ})] C_J \end{aligned} \tag{30}$$

Bringing this quantity back into eq 26, $(\partial/\partial t)\gamma(\mathbf{r},t;\mathbf{R})$ is finally evaluated, whose spatial distribution will be used along with the flux.

3. Proton Transfer in Formamide and Keto−Enol (Amide−Imide) Tautomerization

3.1. Computational Details. ***3.1.1. System Studied.*** We study electron wavepacket dynamics associated with "proton transfer" from enol HO−CR_1═NR_2 to keto O═CR_1−NHR_2 (R_1 = H and R_2 = H) with and without mediation by a water molecule, as depicted in Figure 1. (By "proton transfer", we tentatively mean only the shift of the position of nucleus proton before we decide whether it is really proton transfer or hydrogen-atom migration in the next subsection.) Although the keto form is particularly interesting because it is a unit of the polypeptide, we start from the enol form and then investigate the relations between them through the dynamical analysis of the Pauling resonance structure.

3.1.2. Basis Set, Molecular Orbitals, Configuration State Functions. The electronic wavepackets are determined in an expansion with the configuration state functions (CSFs) of single and double excitations (CISD) with the STO-6G basis set. This basis set is obviously small, but the main concern in this work is not the accuracy but qualitative insight into the dynamical electrons in the course of chemical reactions. The program codes for the SET have been implemented in the GAMESS package.[30]

The 1s-like inner shell orbitals of C, O, and N atoms have been frozen and totally neglected in the process of electronic mixing. Furthermore, in the water-bridging system, the lowest 10 molecular orbitals (MOs) have also been neglected in the SET dynamics, and 1653 CSFs arising from the resultant 25 MOs are actually used. Likewise, for the gas-phase reaction, we have used 1540 CSFs based on 18 MOs. Although we have carried out extensive numerical calculations including several excited states, here we report only the dynamics of the low-energy state starting from the ground electronic state as an initial condition.

3.1.3. Integrators. The nuclear dynamics of eq 6 is carried out with the fifth-order GEAR method.[31] The electronic Hamiltonian and relevant quantities are reconstructed at each time when the nuclear positions are renewed in the above process, and otherwise, the electronic wavepacket is evolved in time with the temporarily fixed electronic Hamiltonian along with the nuclear derivative (momentum) coupling terms X^{k}_{IJ}. Although the electronic and nuclear dynamics should be solved simultaneously, the large difference between their time scales requires us an efficient practice. For instance, the time step to integrate the equations of motion for nuclei and electrons are 10 and 0.2 as, respectively. This uneven propagation is theoretically rationalized in terms of the Trotter decomposition[32] using the two different time steps.

3.1.4. Initial Conditions for the Nuclear Motion. The initial geometry for formamide was set to the enol form, as in Figure 1. The atoms O, C, and N make a molecular plane, and the bridging water molecule is also placed initially so as to lie in that plane. In what follows, we refer to the MOs approximately lying on the plane and to those approximately perpendicular to the plane as σ- and π-orbitals, respectively. Likewise, using only π-orbitals in $\gamma(\mathbf{r},t)$ and $B_{AB}(\mathbf{r},t)$, we estimate the π-electron density and π-bond order, respectively. Similarly, the σ-electron density and σ-bond order are made available. This distinction between the σ- and π-subspaces is just a matter of convenience, and of course, they are not physical observables individually because C_s symmetry is not imposed on the molecular system. On the contrary, all of the vibrational modes are active in the present SET calculations. Because the aim of this study is not to estimate the reaction probability but the mechanism of the electron dynamics associated with proton transfer, we chose

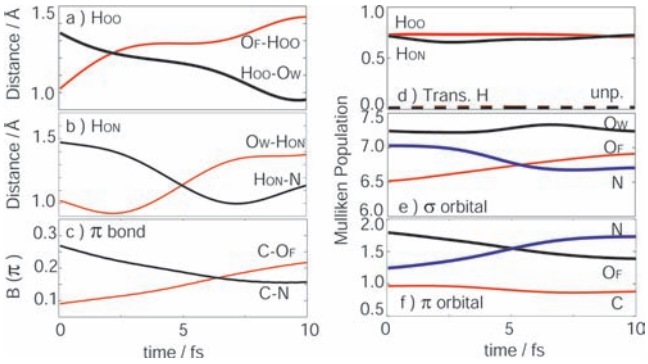

Figure 2. Some selected quantities profiling the time dependence of the water-assisted proton transfer along a reaction pathway. (a) Distance of the transferring proton, H_{OO}, from the neighboring atoms, O_F and O_W. (b) Distance of the transferring proton, H_{ON}, from the neighboring atoms, O_W and N. (c) π-bond order, $B(\pi)$, in two bonds, O_F-C and C−N. (d) Mulliken population on H_{OO} and H_{ON} (solid line and dashed lines represent the number of total electrons and that of the unpaired electrons, respectively.) (e) Mulliken population on the skeletal atoms arising from the σ-orbitals on the molecular plane. (f) Mulliken population on the skeletal atoms arising from the π-orbitals perpendicular to the molecular plane.

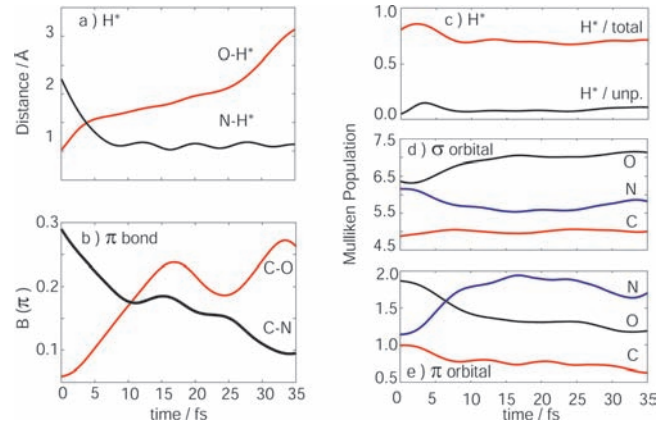

Figure 3. Some selected quantities outlining the time dependence of the forced proton transfer in the gas phase along a reaction pathway. (a) Distance of the transferring proton H* from the neighboring atoms, O_F and O_W. (b) π-bond order, $B(\pi)$, in two bonds, O−C and C−N. (c) Mulliken population and the unpaired electron density on H*. (d) Mulliken population on the skeletal atoms arising from the σ-orbitals on the molecular plane. (e) Mulliken population on the skeletal atoms arising from the π-orbitals.

somewhat artificial initial conditions of nuclear motion to sample as many paths achieving proton transfer as possible.

Gas-Phase Dynamics. We have launched the proton H* in Figure 1 from the minimum energy structure by giving an initial velocity ranging from ∼0.159 to 0.741 Å/fs toward the position of the keto form. Because the potential barrier is high (Markova and Enchev[33] give the potential barrier between the keto and enol forms under the presence of zero, one, and three water molecules; also see the extensive calculations by Wong et al.[34] and Constantino et al.),[35] such high kinetic energies are required for the path to achieve the transfer successfully. Even with these high impact energies, only 4 out of 30 paths actually realized proton transfer.

Water-Assisted Dynamics. We first prepared formamide and water molecule, which are geometrically optimized in each species (not optimized as a supermolecule) and configured them so that the distances between O_W-H_{OO} and $N-H_{ON}$ are both as close as about 1.4 Å. We sampled about 70 paths by scanning the initial velocity of H_{OO}, varying the energy in the antisymmetric stretching vibrational mode of the water molecule and giving or not giving the zero-point energies to the normal modes. Fifty out of these seventy paths have actually reached the proton transfer structure. The potential barrier is of course far lower than that of the gas-phase reaction.[33]

3.2. Proton Transfer in the Ground State: Comparison between Water-Assisted Transfer and Forced Transfer in the Gas Phase. Among the sampled paths chosen as above for the SET, we pick a couple of examples as a generic case study of proton transfer.

3.2.1. Overall Feature of the Reactions. *Water-Assisted Transfer.* We first present the overall feature of an example of the dynamics in water-assisted proton transfer in Figure 2. Panel a indicates the fact that the distance of the proton H_{OO} from O_F becomes longer than that from O_W at a time of about 2 fs, whereas panel b shows that the proton H_{ON} leaves from the site of O_W and arrives at the vicinity of N at about 5 fs. Therefore, the first transfer took place in the site of O_F-O_W, and that of O_F-N followed in this particular example of proton relay. This is not always the case, though. That is, proton transfer in the site of O_W-N can precede that of O_F-O_W. The π-bond order displayed in panel c claims that the double bond has shifted from C−N to O_F-C at a time of about 7 fs. Because the tautomerization is completed in this way, we may judge that the present proton relay has been achieved successfully along this path.

We next survey the basic behavior of the electronic population on the relevant atoms in terms of the Mulliken (electronic) population in panels d−f. In panel d, we notice that the Mulliken population on both H_{OO} and H_{ON} is kept almost constant throughout the course of the transfer process. This clearly indicates that these protons are covered with electrons as much as about 0.7 each. Panel e suggests that the electron density on O_W in the molecular plane remains almost constant, whereas that on O_F (N) increases (decreases) to some extent. Panel f indicates that π-electron density is shifted a little from O_F to N, whereas that on C does not change in the course of the π-bond alternation. We note that this motion of the π-electron density is in the reverse direction to the shift of the position of the π-bond itself.

Forced Transfer in the Gas Phase. To highlight the important feature of the above water-assisted proton transfer, we next survey a reaction path for a forced proton transfer in the gas phase, which is far less favorable energetically. Figure 3 shows the basic behavior of one of such paths. Panel a traces the relative position of H* shifting from the O side to the N area. The variation of the π-bond order in panel b detects a very clear alternation of the double bond from C−N to O−C, and the CN bond becomes single after all. As in the case of water-assisted proton transfer, the proton H* always carries electrons as much as about 0.7. In panel d, we observe an increase (decrease) in electron density of σ-electrons on the atom O (N). The change in the π-electron density on the skeletal atoms behaves more or less similarly to that in the water-assisted proton transfer (panel e to be compared with panel f of Figure 2).

3.2.2. Proton Transfer versus Hydrogen-Atom Migration. In the study of proton transfer dynamics in a collision between H_3O^+ and H_2O, Ushiyama and Takatsuka[17] have observed that the transferring proton is always covered with electrons as much as about 0.6 throughout the collision with the Mulliken population analysis. A similar phenomenon is confirmed for other proton transfer systems in our laboratory. Because the Mulliken population is considerably dependent on the basis set chosen, the amount of electrons carried by the nucleus proton

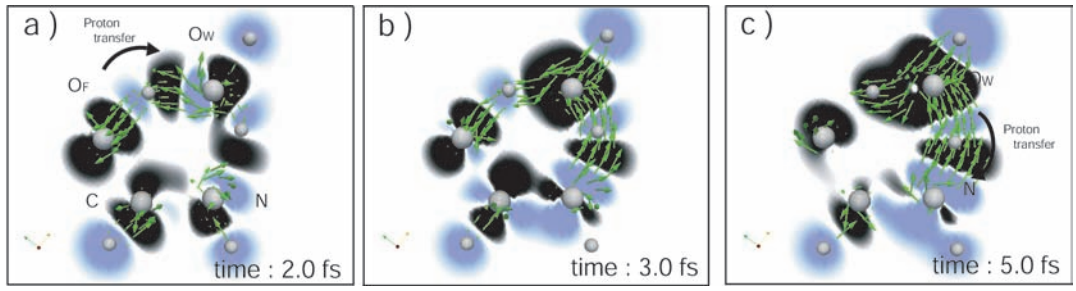

Figure 4. Snapshots of electron flux on the molecular plane arising from σ-orbitals in the course of water-assisted proton transfer dynamics. They are induced mainly in the area connecting the atoms O_F, H_{OO}, O_W, H_{ON}, and N. The time at which the snapshot is taken is indicated in the individual panels. Note that the flow direction is opposite to that of the motion of the protons, and a collective flow covering the entire area of proton transfer is observed. The time-dependent fluctuation of the σ-electron density, estimated with $(\partial/\partial t)\gamma(\mathbf{r},t;\mathbf{R})$ in eq 26, which indicates the increasing (in the black region) and decreasing (in the light-blue region) of σ-electron density.

is not necessarily determined uniquely. Instead of the Mulliken analysis, we have carried out numerical integration to track the amount of electrons around the nucleus proton and found behavior similar to that found with the Mulliken analysis, although a little more fluctuation of the electron density has been observed.[36] This conclusion is consistent with the earlier population analysis based on Bader's theory of atoms in molecules[37] reported by Wong et al.[34] In any analysis, it is commonly concluded that the proton is never transferred as a bare proton in a naked fashion, which is not surprising in view of the high binding energy of the 1s electron in the hydrogen atom, that is 13.6 eV. As described above, the similar phenomenon has been reconfirmed in the present system, where electrons as much as about 0.7 have been found to follow consistently the nucleus proton tightly. Then, the following naive questions arise: Is this "proton transfer" really a proton transfer? If so, in what manner and through which route are such covering electrons rendered back to the proton-launching site. Or, is this process a hydrogen-atom migration in an electron-deficient state? If yes, how and through which route is the additional electron pushed to a destination site? As far as the present system is concerned, chemical intuition suggests that it is unlikely for the hydrogen-atom migration to take place. However, it is certainly critical to confirm whether it is indeed the case because the electronic mechanism of "proton transfer" is closely linked to the electron dynamics of tautomerization.

Therefore, we propose here a rather quantitative condition to distinguish proton transfer and hydrogen-atom migration not by the number of electrons involved but by the qualitative difference in their electronic states. For hydrogen-atom migration, we literally take it as a radical transfer in the hydrogen-atom-like state. As an illustrative example, let us consider a schematic "proton transfer" reaction H−A−B → A−B−H. In the course of this reaction, H radical (H•) should be formed to some large extent in the hydrogen-atom migration. We regard proton transfer to be a concerted rection. That is, it undergoes a transfer through a smooth bond exchange in which an electronic closed-shell structure (α- and β-spin pairing state or simply doubly occupied state irrespective of the number of involved electrons) is realized around the nucleus proton without the formation of radicals. In summary, proton transfer is like a concerted reaction maintaining a closed-shell electronic structure, whereas the hydrogen-atom migration can be termed as a radical or singlet biradical reaction. (Therefore, the closed-shell Hartree−Fock calculation cannot reproduce the state of hydrogen-atom migration in this definition.) We will report in greater detail the account of the theory along with several examples in our future publication.[27]

To monitor the distribution of radicals, or unpaired electrons, at a given atomic site **r** in a molecule, we use the unpaired electron density[21] defined in eqs 12−15. This density was figured out to characterize the nonconcerted (Woodward−Hoffmann forbidden) reactions. Therefore, any indicator to monitor such spatial distribution of unpaired electrons (biradicals) will be equally acceptable. Indeed, several other studies on the unpaired electron have been reported in the theory of chemical reactions proceeding via biradical states.[38−45] In particular, the extensive studies by Davidson and coworkers[38−40] have set a landmark in this field.

In panel d of Figure 2, for the water-bridging system, we have plotted D_A on the two transferring protons. It turns out that both of them remain to be almost zero during the transfer. (Recall that the present SET calculation contains single and double electronic excitations.) Therefore, there is virtually no radical character around the proton, and we conclude on this quantitative basis that this double "proton transfer" is indeed proton transfer. Incidentally, hydrogen-atom migration is frequently observed in reactions of electronically excited states.

As for the forced transfer in the gas phase, we also plot D_A in panel c of Figure 3. Because this is a high barrier process, the radical character is much larger than that of the water-bridging system. Nonetheless, its absolute value is small enough to conclude that this transfer is also proton transfer, although a radical character is a little larger.

3.2.3. Reversal Electron Current against the Proton Motion and Collective Flow through the Bridging Water. Now that we have concluded that the present dynamics are both indeed proton transfer, we next attempt to identify the dynamical electronic flow within the molecular systems associated with the proton transfer. In doing so, we examine the quantum mechanical flux of probability density of electrons, as summarized beforehand in eq 22 in Section 2.2. As readily understood from eq 20, real valued wave functions such as the electronic eigenfunctions in quantum chemistry can give only zero flux. This is simply because the stationary state wave function, which is free of time variable by definition, is a symmetric linear combination of time-forward and -backward waves; thereby the fluxes emerging from each component cancel each other exactly. Therefore, basically, any accurate electronic eigenfunction cannot show how the electrons dynamically flow within a molecule. Our studied electron wavepackets that are given by SET are generally complex valued and include the time variable. Therefore, the electron flux induced by the nuclear kinematic interaction is explicitly calculated.

As for the electron flux on the molecular plane (σ-flux) for the water-bridging system, it is clearly observed in Figure 4

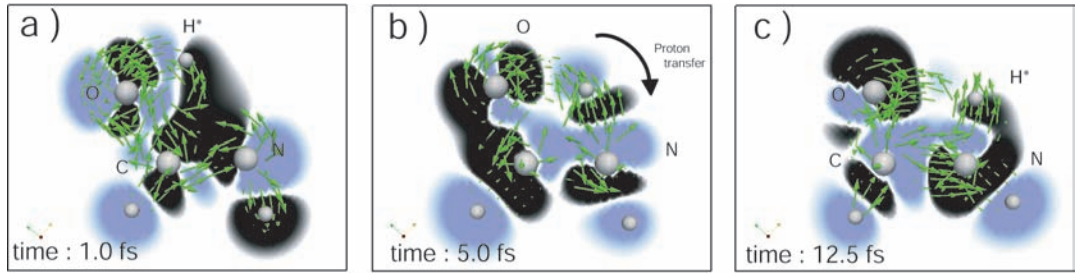

Figure 5. Electron flux on the molecular plane arising from σ-orbitals in the course of gas-phase proton transfer dynamics. They are induced mainly in the area connecting the atoms O_F, H_{OO}, O_W, H_{ON}, and N. The flow direction is mostly opposite to that of the motion of the proton. The time-dependent fluctuation of the σ-electron density, estimated with $(\partial/\partial t)\gamma(\mathbf{r},t;\mathbf{R})$ in eq 26, which indicates the increasing (in black region) and decreasing (in light-blue region) of σ-electron density.

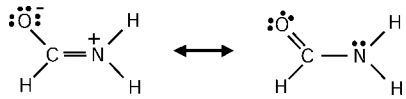

Figure 6. Two dominant resonance forms after the proton transfer.

that the electron flux induced by the nuclear dynamics is flowing in the direction opposite to the proton motion, as though it is compensating the electrons carried by the nucleus proton. In particular, panel b of Figure 4 seems to have a collective electron flow passing through the mediating water molecule. This is the first observation of the electronic backward flux associated with proton transfer.

To augment the physical insight attained through the electronic flux, we study the time derivative of the electron density $(\partial/\partial t)\gamma(\mathbf{r},t;\mathbf{R})$ defined as eq 26. This quantity is positive (negative) if the electron density is increasing (decreasing) at a moment t. Figure 4 shows only the sign of $(\partial/\partial t)\gamma(\mathbf{r},t;\mathbf{R})$ as a function of time and place. It is observed that the areas into which electron flux is flowing are positive. Taking a closer look at the transferring protons, we notice that the electron density in the front side with respect to the proceeding direction tends to be positive, and that in the rear side tends to be negative. In this way, the electrons are pumped to the vicinity of protons and pushed out of the region. Also, for the coexistence of the positive and negative regions around the transferring protons, the Mulliken charge is kept almost constant.

The similar analyses are possible for the forced proton transfer in gas phase, which is displayed in Figure 5. Reflecting the nonsmooth dynamics, which requires much higher initial energy, both the flux and $(\partial)/(\partial t)\gamma(\mathbf{r},t;\mathbf{R})$ look more complicated than in the case of water-assisted system. Nevertheless, one can clearly observe that the electron flux is directed to the opposite side of the proton motion.

3.2.4. Rearrangement of π-Bonds: Dynamical Manifestation of the Pauling Resonance Structures. An electronic state of the zwitterionic form left behind right after the proton transfer, which should be represented in terms of the left-hand-side structure of Figure 6 in the Pauling resonance (valence bond) theory. The corresponding hydrogen-atom migration should leave a biradical state $\dot{O}-\dot{C}H-NH_2$ after the migration and then turn to the keto form. (In fact, however, no such significant unpaired density expected from the above biradical structure has been observed in any instance.) This keto structure $O=CH-NH_2$ is more stable than the zwitterionic structure.[33] Nevertheless, proton transfer rather than hydrogen-atom migration actually took place, as shown above. This fact suggests that the proton transfer is a process of kinetic control and that the bond-breaking to create the hydrogen-atom-like radical state needs a higher energy to surmount.

In the Pauling valence bond theory, however, these two extreme structures are expected to resonate with each other, as shown in Figure 6. The resonance theory is such a useful theory in organic chemistry because it can give the essential feature of the electronic state without quantum mechanical calculation. However, the information provided is essentially static. We therefore investigate the dynamical implication of the resonance structures. First, we consider the bond-order density $B_{AB}(\mathbf{r},t)$ defined in eq 11, which is merely a spatial distribution of the bond order, representing the quality and strength of a chemical bond between atoms A and B. Furthermore, here we concentrate on the π-bond order to track the dynamics of double bonds lying in the region of the skeletal atoms O, C, and N. In Figure 7, panels A−C give a time series of the propagation of the π-bond order, starting from the purely double bond in C−N site right after the proton transfer. Because of the resonance, the double bond penetrates into the O−C site; then, fluctuation of the double bonds continues in between these two sites. (See panels B and C.)

More dramatic time propagation of the π-electron dynamics can be extracted using the flux, as shown in Figure 8. The left column panels provide the flux in a side view (seen in a direction parallel to the molecular plane O−C−N), whereas the right column gives a top view (seen in the direction perpendicular to the molecular plane) of the flux of the same timing. At 2.5 fs (panel a), the electrons are flowing into the vicinity of the C atom from both ends, but at 5.0 fs (panel b), the uniform electron current takes place from left (O side) to right (N side), and at 7.5 fs (panel c), the reverse flow is observed. Furthermore, at 10 fs (panel d), the electrons flow out from the region of the C atom, which the reverse of the flux at 2.5 fs. In this manner, the electron flux continues to fluctuate. Therefore, electron flow behind the resonance theory has been exposed by means of the electron wavepacket dynamics coupled to nuclear motion.

3.2.5. Stabilization of the zwitterionic Resonance Structure by the Mediating Water. Returning to the resonance structures in Figure 6, we immediately notice that the zwitterionic structure may be stabilized far better than the keto structure by polar solvents. In our water-bridging system, a water molecule is already there to mediate proton transfer. After the proton transfer is completed, this water molecule can now serve as a stabilizing polar solvent, as schematically drawn in Figure 9. Such an effect should be much weaker for the keto form. Without the water molecule, the zwitterionic structure is energetically higher than the keto form, but because of the stabilization, their difference turns out to be smaller. This is why the double bonds remain in both sites of O−C and C−N and the π-electron flux continues to fluctuate among these atoms.

To see how crucial the stabilization effect is, we compare it with the forced proton transfer in the gas phase. Panels a−c of

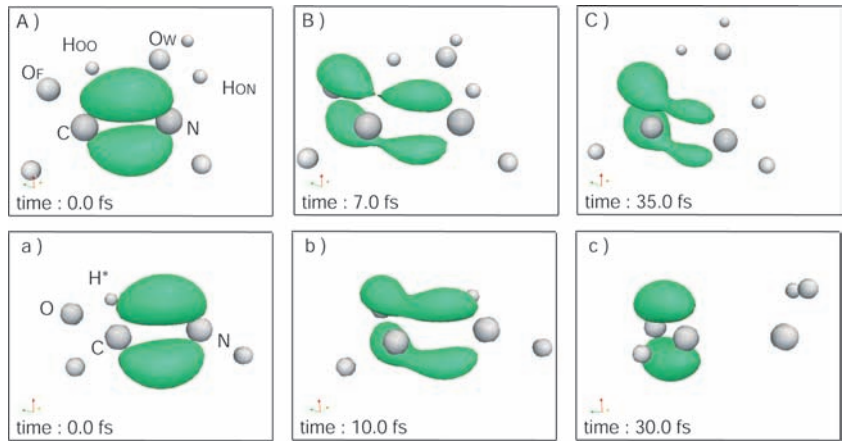

Figure 7. Time propagation of the π-bond order densities in O−C and C−N bonds at each time indicated in the panels. Upper row, panels A−C: the water-assisted proton transfer. Lower row, panels a−c: forced proton transfer in the gas phase. At time 30 fs in the case of the gas-phase reaction, the character of the π-bond between C and N atoms has virtually disappeared, and the pyramidal structure as in the ammonium molecule has shown up around the N atom. The isovalue surfaces on which the bond-order density takes 0.01 are drawn.

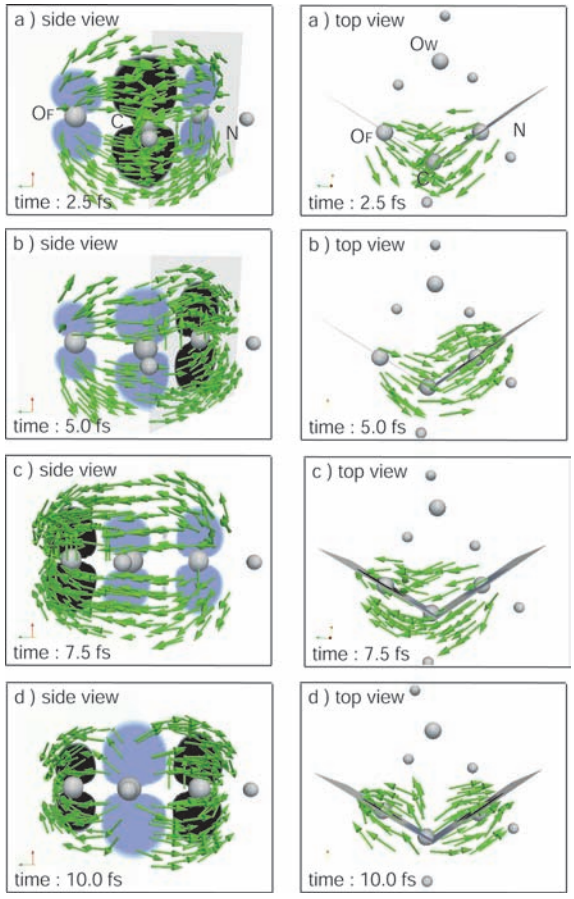

Figure 8. Electron flux arising from π-orbitals in water-assisted proton transfer dynamics at each time indicated in the panels. Left column: a side view parallel to the O−C−N plane. Right column: the top view. In the left column, the time-dependent fluctuation of the π-electron density is shown, which indicates the increasing (in black region) and decreasing (in light-blue region) of π-electron density. In this reaction, a frequent change of the direction of the flux takes place with a period of about several hundred attoseconds.

Figure 7 display the time propagation of the π-bond order. As in the water-assisted proton transfer, the π-bond is first prepared in the C−N site upon proton transfer. It begins to penetrate into the site of O−C, and after some fluctuation time, say 30 fs, it is localized almost completely to O−C, as confirmed in panel c. Furthermore, this panel shows explicitly that the

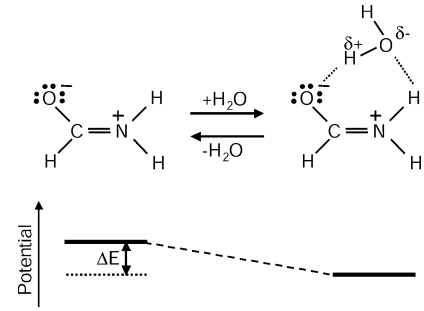

Figure 9. Schematic representation of stabilization of the resonance structure of the zwitterionic form by the bridging water molecule.

bonding state around the nitrogen atom turns out to be triangular-pyramidal ammonium molecule. Therefore, it is virtually not reversible for the double bond at the O−C site to be brought back to the C−N site. The electron flux of the gas-phase system, as exhibited in Figure 10, also supports the one-way propagation of the state. Only the flux directed from the O atom to the N atom through C is observed (up to 11 fs), which is in clear contrast with the fluctuating behavior of Figure 8.

An immediate suggestion from the above study is that the rotation along the axis of C−N in the polypeptide becomes far more difficult by the presence of water molecules for two reasons: They may stabilize the zwitterionic structure as a solvent effect. Water molecules may cause proton relay transfer in the reverse manner of the present state, that is, from keto form (peptide) to enol form, which results in the creation of a strong double bond in C−N. Therefore, the presence of water molecules around the polypeptide can make the dramatic difference from the gas-phase reaction. Although the extent of possibility of free rotation around the C−N bond in polypeptide is well known as one of the classic issues in protein science,[46] one should consider once again these chemical facts in the numerical study of protein folding dynamics.

4. Concluding Remarks

In this article, we have developed a qualitative reaction dynamics and chemical reactivity concept based on the SET, in which dynamical electron wavepackets coupled to nuclear motion are evolved in time. They are expanded in the CSFs. The nuclear kinematic coupling has been explicitly included into the dynamics. In doing so, we proceed from the static theory of chemical reactivity to a dynamical electron theory.

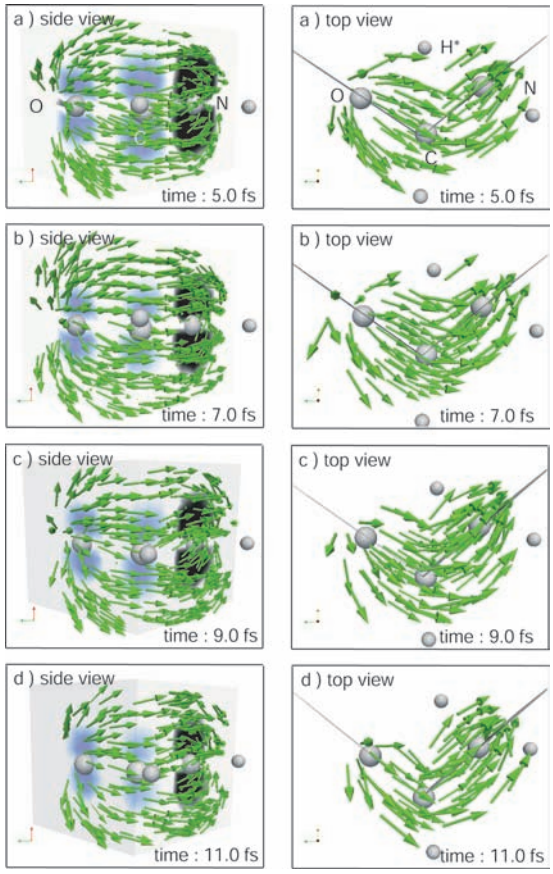

Figure 10. Electron flux arising from π-orbitals in gas-phase proton transfer dynamics at each time indicated in the panels. Left column: a side view parallel to the O−C−N plane. Right column: the top view. In the left column, the time-dependent fluctuation of the π-electron density is shown, which indicates the increasing (in black region) and decreasing (in light-blue region) of π-electron density. In this reaction, the flux does not fluctuate much in direction and is rather unidirectional to the N atomic site.

As such an example, we have investigated the dynamics of water-assisted relayed proton transfer in formamide. We start from the enol form HO−CH═NH and track the transfer process to the keto form O═CH−NH_2. The main findings of the study are as follows. (i) This dynamics has been identified to be indeed a "proton transfer process" rather than hydrogen-atom migration in terms of the unpaired electron density. (ii) We have shown a collective quantum flux of electrons, which flows backward against the proton motion, thereby compensating the electrons tightly covering the proton as represented in terms of the Mulliken charge. (iii) We have revealed the dynamical manifestation of the resonance structures $O^--CH{=}N^+H_2 \leftrightarrow O{=}CH-NH_2$ by means of our dynamical electron theory. The dynamics and relaxation process behind the static view of the resonance theory has been uncovered. (iv) The keto form formamide is one of the simplest species in the group $O{=}CR_1-NHR_2$, which is a unit of polypeptide. In the gas phase, the nitrogen atom may have a pyramidal structure as in the ammonium molecule; therefore, the C−N bond may allow low barrier rotation along it. This rotation is strongly prohibited by the formation of the double bond C═N induced by the proton transfer, which is enhanced by the presence of bridging water molecule.

Therefore, the present dynamical electron theory turns out to be quite useful as a qualitative method for the analysis of chemical reaction dynamics.

Acknowledgment. We thank Dr. Takehiro Yonehara for valuable discussions. This work has been partially supported by a Grant-in-Aid for Scientific Research from the Ministry of Education, Culture, Sports, Science, and Technology in Japan.

References and Notes

(1) Born, M.; Oppenheimer, R. *Ann. Phys.* **1927**, *84*, 457.
(2) De Fazio, D.; Aquilanti, V.; Cavalli, S.; Aguilar, A.; Lucas, J. M. *J. Chem. Phys.* **2008**, *129*, 064303.
(3) Aquilantia, V.; Cappellettib, D.; Pirania, F.; Roncarattia, L. F. *Int. J. Mass Spectrom.* **2009**, *72*, 280.
(4) Hentschel, M.; Kienberger, R.; Spielmann, C.; Reider, G. A.; Milosevi, N.; Brabec, T.; Corkum, C.; Heinzmann, U.; Drescher, M.; Krausz, F. *Nature* **2001**, *414*, 509.
(5) Niikura, H.; Légaré, F.; Hasban, R.; Bandrauk, A. D.; Ivanov, M. Y.; Villeneuve, D. M.; Corkum, P. B. *Nature* **2002**, *417*, 917.
(6) Baltuška, A.; Udem, Th.; Uiberacker, M.; Hentschel, M.; Goulielmakis, E.; Gohle, Ch.; Holzwarth, R.; Yakovlev, V. S.; Scrinzi, A.; Hänsch, A.; Krausz, F. *Nature* **2003**, *421*, 611.
(7) Mairesse, Y.; de Bohan, A.; Frasinski, L. J.; Merdji, H.; Dinu, L. C.; Monchicourt, P.; Breger, P.; Kovacev, M.; Auguste, T.; Carre, B.; Muller, H. G.; Agostini, P.; Salieres, P. *Phys. Rev. Lett.* **2004**, *93*, 163901.
(8) Nabekawa, Y.; Shimizu, T.; Okino, T.; Furusawa, K.; Hasegawa, K.; Yamanouchi, K.; Midorikawa, K. *Phys. Rev. Lett.* **2006**, *96*, 083901.
(9) Carrera, J. J.; Tong, X. M.; Chu, S.-I. *Phys. Rev. A* **2006**, *74*, 023404.
(10) Salamin, Y. I.; Hu, S.; Hatsagortsyan, K. Z.; Keitel, C. H. *Phys. Rep.* **2006**, *427*, 41.
(11) Harumiya, K.; Kawata, I.; Kono, H.; Fujimura, Y. *J. Chem. Phys.* **2000**, *113*, 8953.
(12) Nguyen, N. A.; Bandrauk, A. D. *Phys. Rev. A* **2006**, *73*, 032708, and references cited therein.
(13) Kawata, I.; Kono, H.; Fujimura, Y. *J. Chem. Phys.* **1999**, *110*, 11152.
(14) Yonehara, T.; Takatsuka, K. *J. Chem. Phys.* **2008**, *128*, 154104.
(15) Takatsuka, K.; Yonehara, T. In *Advances in Chemical Physics*; Vol. 144, in press.
(16) Ushiyama, H.; Takatsuka, K. *J. Chem. Phys.* **2001**, *115*, 5903.
(17) Ushiyama, H.; Takatsuka, K. *Angew. Chem., Int. Ed.* **2007**, *46*, 587.
(18) Ushiyama, H.; Takatsuka, K. *Angew. Chem., Int. Ed.* **2005**, *44*, 1237.
(19) Bolton, K.; Hase, W. L.; Peslherbe, G. H. In *Modern Methods for Multidimensional Dynamics Computations in Chemistry*; Thompson, D. L., Ed.; World Scientific: Singapore, 1998; p 143.
(20) Okuyama, M.; Takatsuka, K. *Chem. Phys. Lett.* **2009**, *476*, 109.
(21) Takatsuka, K.; Yamaguchi, K.; Fueno, T. *Theor. Chim. Acta* **1978**, *48*, 175.
(22) Jasper, A.; Kendrick, B. K.; Mead, C. A.; Truhlar, D. G. Chapter 8. In *Modern Trends in Chemical Reaction Dynamics; Part I*; Yang, X., Liu K., Eds.; World Scientific: Singapore, 2004.
(23) Amano, M.; Takatsuka, K. *J. Chem. Phys.* **2005**, *122*, 084113.
(24) Takatsuka, K. *J. Phys. Chem. A* **2007**, *111*, 10196.
(25) Yonehara, T.; Takatsuka, K. *J. Chem. Phys.* **2008**, *129*, 134109.
(26) Yonehara, T.; Takahashi, S.; Takatsuka, K. *J. Chem. Phys.* **2009**, *130*, 214113.
(27) Nagashima K.; Takatsuka, K., to be published.
(28) Schiff L. I. *Quantum Mechanics*; McGraw-Hill: New York, 1968.
(29) (a) Löwdin, P.-O. *Phys. Rev.* **1955**, *97*, 1474. (b) McWeeny, R. *Proc. R. Soc. London, Ser. A* **1954**, *232*, 114.
(30) Schmidt, M. W.; Baldridge, K. K.; Boatz, J. A.; Elbert, S. T.; Gordon, M. S.; Jensen, J. H.; Koseki, S.; Matsunaga, N.; Nguyen, K. A.; Su, S. J. *J. Comput. Chem.* **1993**, *14*, 1347.
(31) Press, W.; Teukolsky, S. A.; Vetterling, W. T.; Flannery, B. P. *Numerical Recipes*; Cambridge University Press: Cambridge, U.K., 1992.
(32) Schulman L. S. *Techniques and Applications pf Path Integratin*; John Wiley: New York, 1981.
(33) Markova, N.; Enchev, V. *THEOCHEM* **2004**, *679*, 195.
(34) Wong, M. W.; Wiberg, K. B.; Frisch, M. J. *J. Am. Chem. Soc.* **1992**, *114*, 1645.
(35) Constantino, E.; Solans-Monfort, X.; Sodupe, M.; Bertran, J. *Chem. Phys.* **2003**, *295*, 151.
(36) Nagashima K.; Takatsuka, K., unpublished data.
(37) Bader, R. F. W. *Acc. Chem. Res.* **1985**, *9*, 18.
(38) Staroverov, V. N.; Davidson, E. R. *Chem. Phys. Lett.* **2000**, *330*, 161.
(39) Staroverov, V. N.; Davidson, E. R. *J. Am. Chem. Soc.* **2000**, *122*, 186.
(40) Staroverov, V. N.; Davidson, E. R. *J. Am. Chem. Soc.* **2000**, *122*, 7377.

(41) Lain, L.; Torre, A.; Bochicchio, R. C.; Ponec, R. *Chem. Phys. Lett.* **2001**, *346*, 283.
(42) Torre, A.; Lain, L. *J. Phys. Chem. A* **2003**, *107*, 127.
(43) Head-Gordon, M. *Chem. Phys. Lett.* **2003**, *372*, 508.
(44) Lobayan, R. M.; Bochicchio, R. C.; Lain, L.; Torre, A. *J. Chem. Phys.* **2005**, *123*, 144116.
(45) Proynov, E. I. *THEOCHEM* **2006**, *159*, 762.
(46) Liu, T.; Li, H.; Huang, M.-B.; Duan, Y.; Wang, Z.-X. *J. Phys. Chem. A* **2008**, *112*, 5436.

JP905583S